J|A|C|S
COMMUNICATIONS

Published on Web 11/27/2003

Stereochemically Controlled PMMA-Exfoliated Silicate Nanocomposites Using Intergallery-Anchored Metallocenium Cations

Wesley R. Mariott and Eugene Y.-X. Chen*

Department of Chemistry, Colorado State University, Fort Collins, Colorado 80523-1872

Received September 15, 2003; E-mail: eychen@lamar.colostate.edu

Nanocomposites consisting of continuous polymer matrixes reinforced by a few weight percent of intercalated or exfoliated layered silicate nanofillers have attracted increasing attention in recent years due to their unique materials properties.[1] As an important member of such advanced materials, poly(methyl methacrylate) (PMMA)-clay nanocomposites exhibit enhanced thermal stability and flame retardancy, increased storage modulus and glass transition temperature (T_g), and improved toughness and barrier properties.[2] However, the PMMA matrixes present in the previous nanocomposites were essentially atactic and produced from various radical polymerization processes.[2] The physical and mechanical properties of a polymer having stereocenters in the repeating unit depend largely on its stereochemistry; stereoregular polymers typically have superior materials properties such as solvent resistance, modulus, impact strength, and fatigue resistance compared to their amorphous counterparts. Therefore, the study of structure−property relationships of the nanocomposite using stereochemically controlled PMMA is of fundamental interest.

Although the stereospecific polymerization of MMA with group 4 metallocenes has been well documented,[3] the synthesis of PMMA−silicate nanocomposites using these catalysts remains unexplored. If such stereospecific metal complexes in their active form can be effectively anchored in the silicate galleries, subsequent polymerization should lead to PMMA with the desired stereomicrostructures. However, the challenge in catalyst intercalation lies in the incompatibility between these often highly sensitive metal catalysts and unprotected layered silicate galleries that often contain protic impurities and polar functionalities. Nevertheless, Cp_2ZrMe^+ was reported to directly ion-exchange into the galleries of the synthetic silicates after the internal surfaces were protected with methylalumoxane.[4] The more tolerant late metal (Pd)-based olefin polymerization catalyst was intercalated in the unprotected fluorohectorite galleries.[5] We communicate here the synthesis and characterization of intergallery-anchored metallocenium cations via a non-cation-exchange approach involving protonolysis of the metallocene dimethyl with $Me(HT)_2NH^+$/MMT, a montmorillonite (MMT) clay modified by methyl bis(hydrogenated tallow alkyl) ammonium. These intercalated metallocene catalysts allow for the first synthesis of in situ polymerized nanocomposites comprising delaminated silicate nanoplatelets dispersed in the atactic, isotactic, or syndiotactic PMMA matrixes.

The reactions of the predried $Me(HT)_2NH^+$/MMT with C_{2v}-symmetric Cp_2ZrMe_2, C_2-symmetric *rac*-(EBI)$ZrMe_2$ (EBI = $Et(Ind)_2$), and C_s-symmetric $CGCTiMe_2$ (CGC = $Me_2Si(Me_4C_5)$-(*t*-BuN)) proceed quantitatively to generate the intercalated metallocenium catalysts Cp_2ZrMe^+/MMT, *rac*-(EBI)$ZrMe^+$/ MMT, and $CGCTiMe^+$/MMT, respectively (Chart 1),[6] after elimination of methane and discharge of the resulting neutral amine. A slight excess of the metallocene dimethyl and the discharged neutral amine were effectively removed by extensive washing with toluene and hexanes followed by drying under vacuum, as monitored by ^1H NMR spectra of the filtrate residue. In addition to the ^1H NMR evidence,[6] the X-ray photoelectron spectroscopy (XPS) analysis of the synthesized zirconocenium cation-intercalated silicates showed the absence of any N peaks, strongly suggesting that the protonolysis reaction followed by the neutral amine discharge was quantitative and that decomposition or side reactions (e.g., surface absorption) involving the metallocene dimethyl was negligible.

Chart 1

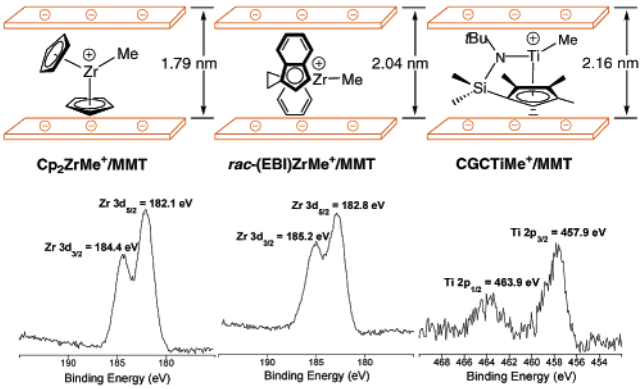

On the basis of the powder X-ray diffraction (XRD) analysis, the basal spacings for the synthesized Cp_2ZrMe^+/MMT, *rac*-(EBI)-$ZrMe^+$/ MMT, and $CGCTiMe^+$/MMT are 1.79, 2.04, and 2.16 nm, respectively (Chart 1, Figure 1), all of which differ substantially from that of precursor $Me(HT)_2NH^+$/MMT (2.33 nm). The increased *d* spacing from Cp_2ZrMe^+/MMT to *rac*-(EBI)$ZrMe^+$/MMT is consistent with the relative molecular dimensions of the zirconocenium cations; however, $CGCTiMe^+$/MMT has the largest *d* spacing in this series, presumably reflecting the weaker coordination between the titanocenium cation and the anionic silicate sheets.

The formation of the metallocenium cations is further confirmed by the high-resolution XPS analyses. Consistent with the binding energy for Cp_2ZrMe^+ (generated by mixing Cp_2ZrMe_2 with methylalumoxane) obtained by Gassman,[7] the measured Zr $3d_{5/2}$ binding energy for Cp_2ZrMe^+/MMT is 182.1 eV (Chart 1), which is 1.4 eV higher than that of Cp_2ZrMe_2. Likewise, the measured Zr $3d_{5/2}$ binding energy for *rac*-(EBI)$ZrMe^+$/MMT is 182.8 eV, which is 0.8 eV higher than that of *rac*-(EBI)$ZrCl_2$[8] and estimated to be ~1.8 eV higher than that of *rac*-(EBI)$ZrMe_2$, after considering the fact that dimethyl zirconocene has ~1.0 eV lower binding energy than that of the dichloride derivative.[7] Finally, the measured Ti $2p_{3/2}$ binding energy for $CGCTiMe^+$/MMT is 457.9 eV; this value is 1.0 eV higher than that of $CGCTiMe_2$. These results strongly suggest that the metallocene complexes anchored inside the galleries of MMT are in their respective cationic forms.

The polymerizations of MMA catalyzed by Cp_2ZrMe^+/MMT, *rac*-(EBI)$ZrMe^+$/ MMT, and $CGCTiMe^+$/MMT produced atactic ([mr] = 39.8%), isotactic ([mm] = 93.0%), and syndiotactic ([rr] = 72.0%) PMMA−silicate nanocomposites, respectively (Table 1).

10.1021/ja038522c CCC: $25.00 © 2003 American Chemical Society

Table 1. Results of MMA Polymerization and Properties of PMMA−Silicate Nanocomposites[a]

entry	catalyst	solvent	time (h)	yield (%)	M_n[b] (kg/mol)	PDI[b]	T_g[c] (°C)	T_{max}[d] (°C)	$T_{int,end}$[e] (°C)	[mm][f] (%)	[mr][f] (%)	[rr][f] (%)
1	Cp_2ZrMe^+/MMT	toluene	24	38	45.1	1.46	103	371	325, 393	24.5	39.8	35.7
2	*rac*-(EBI)$ZrMe^+$/MMT	toluene	3	80	102	1.58	64	371	328, 405	93.0	4.7	2.3
3	CGCTiMe^+/MMT	toluene	24	36	98.9	1.47	128	367	323, 388	4.8	23.2	72.0
4[g]	CGCTiMe^+/MMT	toluene	24	44	130	1.29	126	370	320, 392	3.9	25.0	71.1
5	CGCTiMe^+/MMT	DCB	24	85	182	1.37	126	368	328, 392	2.9	23.9	73.2

[a] Carried out in an argon-filled glovebox (oxygen and moisture <1.0 ppm) at room temperature and in toluene or DCB (*o*-dichlorobenzene); intercalated clay catalyst loading vs monomer: 5 wt %. [b] Number-average molecular weight (M_n) and polydispersity index (PDI) determined by GPC relative to PMMA standards. [c] Glass transition temperature determined by DSC from second scans. [d] dwt %/d*T* peak max for maximum rate decomposition temperature determined by TGA. [e] Decomposition onset temperatures determined by TGA. [f] Methyl triads determined by ^{1}H NMR spectroscopy. [g] The catalyst was preswelled in toluene overnight before the addition of MMA.

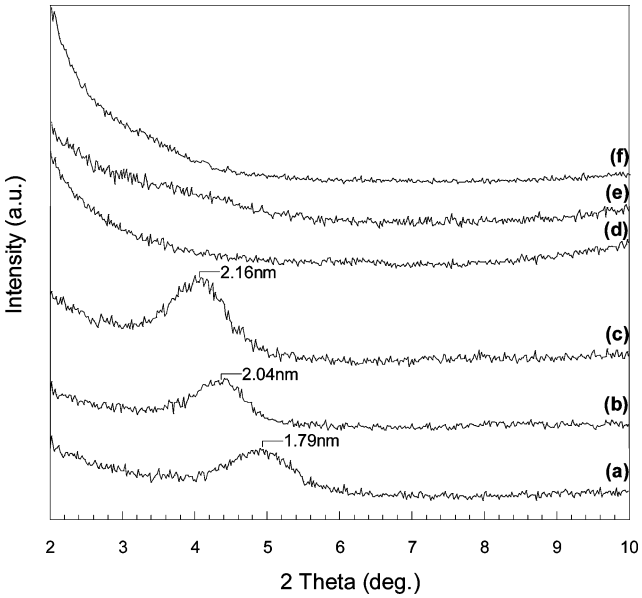

Figure 1. Overlay of XRD plots for Cp_2ZrMe^+/MMT (a), *rac*-(EBI)$ZrMe^+$/MMT (b), CGCTiMe^+/MMT (c), *a*-PMMA/MMT (d), *i*-PMMA/MMT (e), and *s*-PMMA/MMT (f).

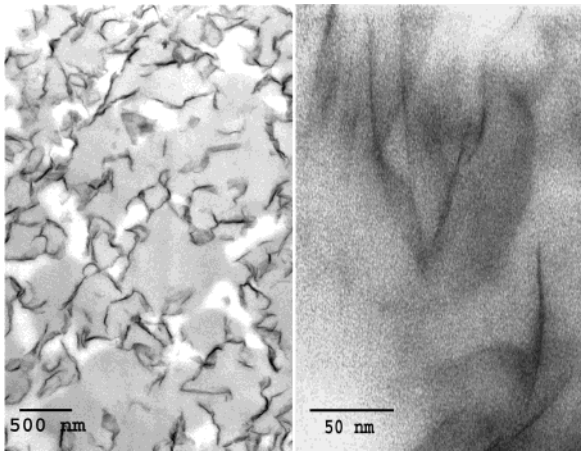

Figure 2. TEM images of *i*-PMMA/MMT nanocomposite.

The most significant property difference among these three nanocomposites varying in the polymer matrix stereochemistry is the T_g: 128 °C for *s*-PMMA/MMT, 103 °C for *a*-PMMA/MMT, and 64 °C for *i*-PMMA/MMT (which is ∼10 °C higher than that for the pure *i*-PMMA of the same isotacticity). The powder XRD (Figure 1) showed complete absence of diffraction peaks at $2\theta = 2-10°$ for all three types of PMMA nanocomposites produced, which is indicative of exfoliated structures. The exfoliated morphology of the isotactic PMMA−silicate nanocomposite produced by *rac*-(EBI)$ZrMe^+$/MMT was further examined and confirmed by transmission electron microscopy (TEM) analyses (Figure 2). The low magnification (500-nm scale bar) image shows homogeneous clay dispersion, whereas the high magnification (50-nm scale bar) image demonstrates exfoliation of the silicate nanoplatelets.

In conclusion, we report the first synthesis and characterization of stereochemically controlled PMMA−silicate nanocomposites using the intergallery-anchored metallocenium cations. The access to such nanocomposites allows for fundamental studies of polymer stereochemistry effect on nanocomposite properties; efforts directed toward this goal are currently underway.

Acknowledgment. This work was supported by Colorado State University. E.Y.C. gratefully acknowledges an Alfred P. Sloan Research Fellowship.

Supporting Information Available: Experimental details, XPS spectra, and TEM images (PDF). This material is available free of charge via the Internet at http://pubs.acs.org.

References

(1) For recent reviews, see: (a) *Polymer Nanocomposites: Synthesis, Characterization, and Modeling*; Krishnamoorti, R., Vaia, R. A., Eds.; ACS Symposium Series 804; American Chemical Society: Washington, DC, 2001, and references therein. (b) *Polymer-Clay Nanocomposites*; Pinnavaia, T. J., Beall, G. W., Eds.; Wiley: New York, 2000, and references therein. (c) Alexandre, M.; Dubois, P. *Mater. Sci. Eng., R.* **2000**, *28*, 1−63. (d) Giannelis, E. P.; Krishnamoorti, R.; Manias. *Adv. Polym. Sci.* **1999**, *138*, 107−147.

(2) For recent examples, see (a) Su, S.; Wilkie, C. A. *J. Polym. Sci., Part A: Polym. Chem.* **2003**, *41*, 1124−1135. (b) Fan, X.; Xia, C.; Advincula, R. C. *Polym. Prepr.* **2003**, *44*, 1099−1100. (c) Wang, D.; Zhu, J.; Yao, Q.; Wilkie, C. A. *Chem. Mater.* **2002**, *14*, 3837−3843. (d) Huang, X.; Brittain, W. J. *Macromolecules* **2001**, *34*, 3255−3260. (e) Zeng, C.; Lee, J. L. *Macromolecules* **2001**, *34*, 4098−4103. (f) Choi, Y. S.; Choi, M. H.; Wang, K. H.; Kim, S. O.; Kim, Y. K.; Chung, I. J. *Macromolecules* **2001**, *34*, 8978−8985. (g) Bandyopadhyay, S.; Hsieh, A. J.; Giannelis, E. P. In *Polymer Nanocomposites: Synthesis, Characterization, and Modeling*; Krishnamoorti, R., Vaia, R. A., Eds.; ACS Symposium Series 804; American Chemical Society: Washington, DC, 2001, pp 15−25. (h) Bandyopadhyay, S.; Giannelis, E. P.; Hsieh, A. J. *Polym. Mater. Sci. Eng.* **2000**, *82*, 208−209.

(3) (a) Jin, J.; Mariott, W. R.; Chen, E. Y.-X. *J. Polym. Sci., Part A: Polym. Chem.* **2003**, *41*, 3132−3142. (b) Chen, E. Y.-X.; Cooney, M. J. *J. Am. Chem. Soc.* **2003**, *125*, 7150−7151. (c) Karanikolopoulos, G.; Batis, C.; Pitsikalis, M.; Hadjichristidis, N. *Macromol. Chem. Phys.* **2003**, *204*, 831−840. (d) Bolig, A. D.; Chen, E. Y.-X. *J. Am. Chem. Soc.* **2002**, *124*, 5612−5613. (e) Frauenrath, H.; Keul, H.; Höcker, H. *Macromolecules* **2001**, *34*, 14−19. (f) Cameron, P. A.; Gibson, V.; Graham, A. J. *Macromolecules* **2000**, *33*, 4329−4335. (g) Nguyen, H.; Jarvis, A. P.; Lesley, M. J. G.; Kelly, W. M.; Reddy, S. S.; Taylor, N. J.; Collins, S. *Macromolecules* **2000**, *33*, 1508−1510. (h) Deng, H.; Shiono, T.; Soga, K. *Macromolecules* **1995**, *28*, 3067−3073. (i) Collins, S.; Ward, D. G.; Suddaby, K. H. *Macromolecules* **1994**, *27*, 7222−7224.

(4) Tudor, J.; Willington, O'Hare, D.; Royan, B. *Chem. Commun.* **1996**, 2031−2032.

(5) Bergman, J. S.; Chen, H.; Giannelis, E. P.; Thomas, M. G.; Coates, G. W. *Chem. Commun.* **1999**, 2179−2180.

(6) See Supporting Information for experimental details.

(7) Gassman, P. G.; Callstrom, M. R. *J. Am. Chem. Soc.* **1987**, *109*, 7875−7876.

(8) Atiqullah, M.; Faiz, M.; Akhtar, M. N.; Salim, M. A.; Ahmed, S.; Khan, J. H. *Surf. Interface Anal.* **1999**, *27*, 728−734.

JA038522C